PAPER

Design of a thermally stable succinonitrile mechanophore featuring electron-withdrawing triazine rings for radical polymerization

Hajime Sugita,[a] Akira Kodaka,[a] Akira Takahashi, [ID] [a] Koichiro Mikami*[b] and Hideyuki Otsuka [ID] *[a,c]

A novel, triazine ring-containing succinonitrile-based mechanophore was designed and synthesized through radical stabilization energy calculations and molecular simulations. This mechanophore exhibits higher thermal stability than a classical mechanophore and a clear mechanochromic response *via* C–C bond cleavage. This enables its incorporation into polymers *via* radical polymerization. This study advances the design of thermally stable mechanophores and provides new insights into the relationship between structures and properties in radical-based mechanochemistry, offering new opportunities in polymer chemistry.

Introduction

Over the past two decades, various materials containing mechanophores that respond to mechanical energy have been developed. These materials exhibit novel functional properties such as self-healing,[1–3] self-reinforcing,[4,5] and damage detection,[6–10] as well as the ability to release small molecules.[11–17] The development of mechanophores is a central avenue of research in the field of mechanoresponsive materials.[18–20] For example, mechanophores can induce color changes or fluorescence in materials.[21] They can also enable the release of small molecules such as acids,[22,23] carbocations,[8,24–26] and ketenes[27] through chemical reactions in response to mechanical forces.

We have developed a series of radical-type mechanophores (RMs) that undergo homolytic cleavage of the central C–C bond under mechanical force to generate radical species.[28–34] These species significantly affect the properties of the resulting materials.[5,35–44] One drawback of RMs is their high tendency to dissociate under ambient conditions, which hinders the application of living radical polymerization techniques and the further development of mechanochromic materials. However, we have demonstrated that substituent effects on the resulting radicals can control the stability of the central C–C bond.[33,34] For example, introducing electron-withdrawing groups (EWGs) such as pyridine or triazine rings at the 9-position of fluorene-based mechanophores greatly improves thermal stability and prevents dissociation under ambient conditions, compared to a phenyl group.[33]

Herein, we report the synthesis and mechanochemical reactivity of a bistriazinyldiarylsuccinonitrile (BTASN)-type mechanophore, in which triazine rings serve as EWGs instead of phenyl groups in tetraarylsuccinonitrile (TASN), one of the most extensively studied RMs to date (Scheme 1). BTASN is a
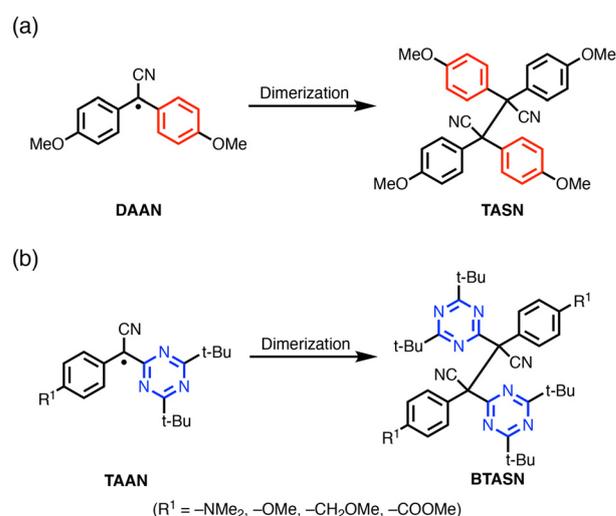
Scheme 1 Chemical structures of radicals and the corresponding RMs: (a) TASN-type mechanophore and (b) BTASN-type mechanophores investigated in this work with −NMe₂, −OMe, −CH₂OMe, and −COOMe substituents.

[a]Department of Chemical Science and Engineering, Institute of Science Tokyo, Meguro-ku, Tokyo 152-8550, Japan. E-mail: otsuka@mct.isct.ac.jp
[b]Engineering Division, Process Device Innovation Center, Panasonic Industry Co., Ltd, 1006 Kadoma, Kadoma City, Osaka 571-8506, Japan. E-mail: mikami.koichiro@jp.panasonic.com
[c]Research Center for Autonomous Systems Materialogy (ASMat), Institute of Integrated Research, Institute of Science Tokyo, 4259 Nagatsuta-cho, Midori-ku, Yokohama, Kanagawa 226-8501, Japan

TASN derivative in which two of the aryl groups are triazine rings; it is a dimer of triazinylarylacetonitrile (TAAN) radicals, whereas typical TASN compounds are dimers of diarylacetonitrile (DAAN) derivatives. The presence of triazine rings as EWGs adjacent to the sp^2-hybridized carbon radical center, flanked by two aromatic rings, is expected to significantly enhance the thermal stability of the RMs. This approach enables the design of new TASN-type mechanophores with high thermal tolerance and facilitates the synthesis of materials *via* living radical polymerization.

Results and discussion

Computational studies

Before synthesizing BTASN, we investigated the substitution effects on its dissociation behavior by calculating the radical stabilization energy (RSE), which reflects the thermodynamic stability of radicals, and by performing constrained geometry simulating external force (CoGEF) calculations,[45,46] which can simulate the cleavage of the bond through mechanical force and allow theoretical evaluation of mechanochemical reactivity (Fig. 1). In our previous study, we demonstrated that the thermal tolerance of a series of RMs with the same molecular skeleton can be explained by the relationship between two key parameters: the RSE value and the Hammett or modified

Swain–Lupton constant at the *para* position (σ_p).[34] As expected, the RSE values decreased in the order –COOMe (−142.27 kJ mol^{-1}), –CH$_2$OMe (−145.46 kJ mol^{-1}), –OMe (−153.40 kJ mol^{-1}), and –NMe$_2$ (−164.49 kJ mol^{-1}), correlating with increasing σ_p values (Fig. 1a), showing a trend similar to that observed for TASNs.[34] The values were clearly lower than those of TASNs (Table S3, please see also the section Revisit of RSE *vs.* Hammett constant and its scope and limitation). The CoGEF calculations further revealed that the mechanical elongation of BTASN leads to bond cleavage at the central C–C bond. The F_{max} values obtained for **BTASN-COOMe**, **BTASN-CH$_2$OMe**, **BTASN-OMe** and **BTASN-NMe$_2$** were 4.61, 4.56, 3.94 and 3.66 nN, respectively (Fig. 1b and S40), following the same trend as the RSE. Considering that the F_{max} value of TASN is 4.54 nN,[46] **BTASN-OMe** is expected to exhibit greater thermal stability and mechanoresponsiveness.

Molecular dynamics (MD) simulations at the single-molecular level supported this scenario. Canonical ensemble (NVT) calculations were performed for atactic PMMA pentamers grown from bifunctional atom transfer radical polymerization (ATRP) initiators containing **BTASN-OMe** and **TASN**, using a universal neural network potential.[47,48] The simulations were performed by incrementally increasing the external force applied to the terminal carbon atoms in 0.01 nN steps, from 0.2 to 0.3 nN. For **BTASN-OMe-PMMA5mers**, homolytic cleavage of the central C–C bond occurred uniformly at 0.23 nN (Fig. S42 and Movies 1, 2). As we expected, the same bond in **TASN-PMMA5mers** was also cleaved at 0.23 nN (Fig. S43 and Movies 3, 4), indicating that **BTASN-OMe** exhibits not only enhanced thermal stability but also mechanoresponsiveness comparable to that of **TASN**. Based on these theoretical findings and the ease of synthetic accessibility, we proceeded to prepare **BTASN-OMe**-based RMs.

### Synthesis and thermal tolerance study

Scheme 2 shows the synthetic procedure for **BTASN-OMe** and its corresponding bifunctional ATRP initiator. A copper-catalyzed cross-coupling reaction was employed to introduce two *tert*-butyl groups onto the triazine ring (75%).[49] Nucleophilic substitution of 1-chloropropanol afforded compound **1** (85%). Protection of the hydroxy group in **1** with a *tert*-butyldimethylsilyl (TBS) group gave compound **2** (96%). The introduction of the di-*tert*-butyltriazine ring to the TBS-protected intermediate afforded **3** (94%). Dimerization of **3** using K$_3$[Fe(CN)$_6$] and 1,8-diazabicyclo[5.4.0]undec-7-ene (DBU) yielded **4**, the BTASN mechanophore core (88%). Subsequent deprotection of TBS groups under acidic conditions (90%) furnished the diol (**BTASN-OH**), which was then esterified with 2-bromoisobutyryl bromide to afford the desired bifunctional ATRP initiator, **BTASN-Int** (50%).

To evaluate the thermal tolerance of **BTASN-OH**, variable-temperature electron paramagnetic resonance spectroscopy (VT-EPR) measurement was performed in anisole solution (Fig. 2). Measurements at elevated temperatures revealed the formation of dissociated radical species with a *g* value of 2.003, which was absent at 25 °C (Fig. S35), consistent with the
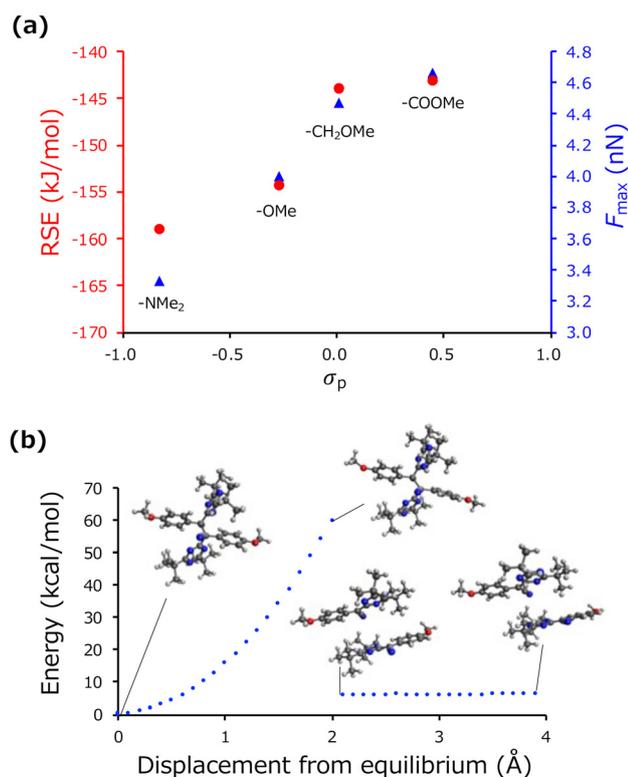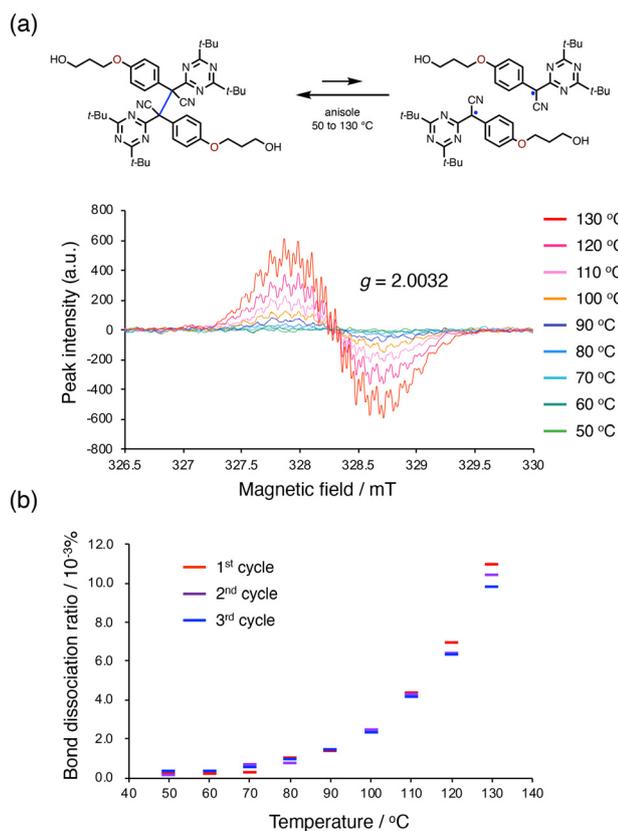

Fig. 1 (a) σ_p values *versus* RSE and F_{max} of **BTASN-COOMe**, **BTASN-CH$_2$OMe**, **BTASN-OMe**, and **BTASN-NMe$_2$**. (b) CoGEF calculation result of **BTASN-OMe** (unrestricted B3LYP/6-31G(d,p)).
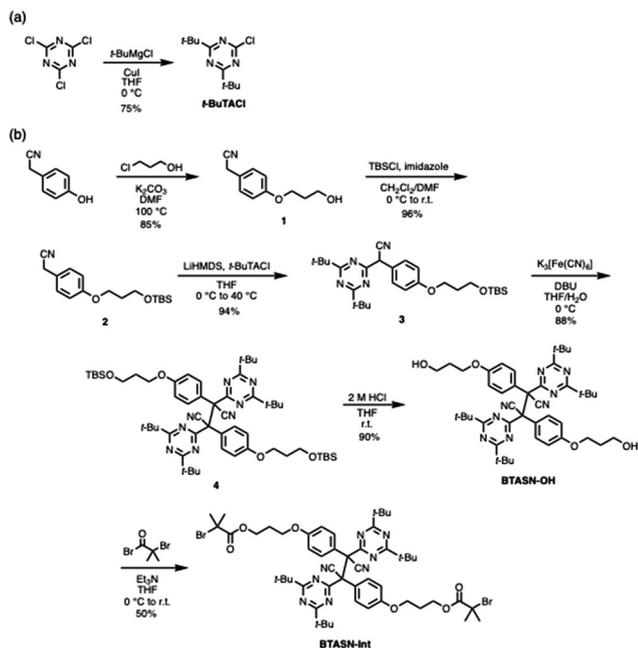
**Scheme 2** Synthetic scheme of (a) *t*-BuTACl and (b) BTASN-OMe derivatives.

Fig. 2 (a) VT-EPR spectra of **BTASN-OH** in anisole. (b) The plot of the temperature-dependent dissociation ratio.

generation of carbon-centered radicals. The dissociation ratio of the central C–C bond increased with increasing temperature. The dissociation ratio of **BTASN-OH** at 100 °C was estimated to be 2.5×10^{-3}%, whereas that of **TASN** under the same conditions was 0.16%,[29,31] approximately 64 times higher than that of **BTASN-OH**. These results indicate that, as expected, the triazine ring substantially enhances the thermal stability of TASN-based RMs, similar to previous observations for fluorene-type RMs,[32] due to its strong electron-withdrawing character.

ATRP of MMA using the bifunctional initiator

Due to the low thermal stability of the central C–C bonds in tetraaryl-type mechanophores, the TASN skeleton has been incorporated into polymeric materials through polyaddition, click reactions, sol–gel reactions, and cationic ring-opening polymerization to avoid radical processes.[29,31,36,37,50–59] In contrast, the superior thermal stability of **BTASN** enables its introduction into polymer structures using conventional radical polymerization techniques. ATRP of methyl methacrylate (MMA) using **BTASN-Int** as the initiator was carried out in toluene at 35 °C (MMA/**BTASN-Int**/CuBr/CuBr$_2$/dNbpy = 940/1/2/0.4/5). This was followed by dehalogenation of the polymer chain ends to prevent the terminal halogen atom from being extracted by the radicals generated by mechanical force (Scheme 3a). The number-average molecular weight (M_n) and
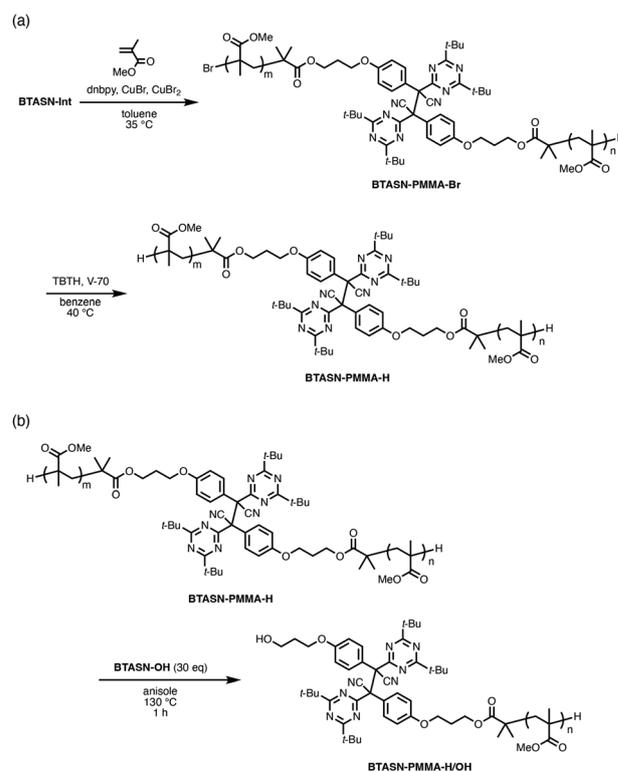

Scheme 3 (a) Synthetic scheme of ATRP of MMA using the bifunctional initiator consisting of **BTASN** followed by dehalogenation of the polymer chain ends. (b) Radical exchange reaction between **BTASN-PMMA-H** and **BTASN-OH**.

dispersity (M_w/M_n) of the resulting PMMA, determined by gel permeation chromatography (GPC) in THF, were M_n (RI) = 16 000 g mol^{-1} and M_w/M_n = 1.08. To confirm whether ATRP initiated from **BTASN-Int** and proceeded in a bifunctional manner, a radical exchange reaction between the resulting polymer and excess **BTASN-OH** was performed at 130 °C for 1 h (Scheme 3b). After the exchange reaction, the M_n value of the polymer was reduced to nearly half of its original value, while the dispersity remained narrow (M_n = 9790, M_w/M_n = 1.10; Fig. 3a, red line). This result confirms that the polymerization proceeded as designed, affording the desired polymer product (**BTASN-PMMA-H**) with a BTASN unit located at the center of the main chain.
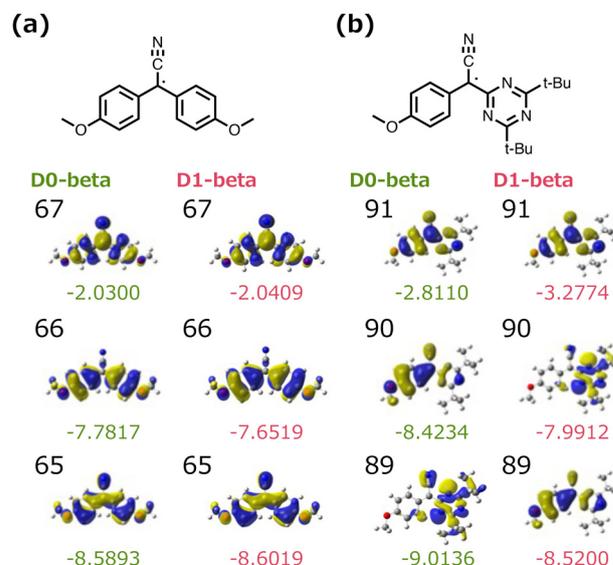
Mechanoresponsive studies

To investigate the mechanical responsiveness of **BTASN-PMMA-H**, a grinding test was performed at room temperature using a ball mill (30 Hz, 10 min). The originally white powder turned pink after grinding (Fig. 3b). EPR measurement of the ground powder clearly showed a signal corresponding to the carbon-centered radicals (g = 2.003), attributed to the homolytic cleavage of the central C–C bond in the mechanophore (Fig. 3c). The mechanically induced bond dissociation ratio (BDR) was found to be 2.5% for BTASN, which is on the same order of magnitude as that of **TASN** (5.1%).[29] In contrast, as shown in Fig. 2, the thermal dissociation ratio of **BTASN-OH** was approximately 64 times lower than that of **TASN**.[31] Solid-state UV-vis spectroscopy of the ground sample revealed a new absorption peak at 550 nm, along with increased absorbance across the broad visible region (Fig. 3d), both attributed to the BTASN-derived radical species. These results are in good agreement with theoretical predictions, indicating that the triazine ring, acting as an electron-withdrawing group, imparts enhanced thermal stability to the mechanophore while retaining its mechanochemical reactivity.
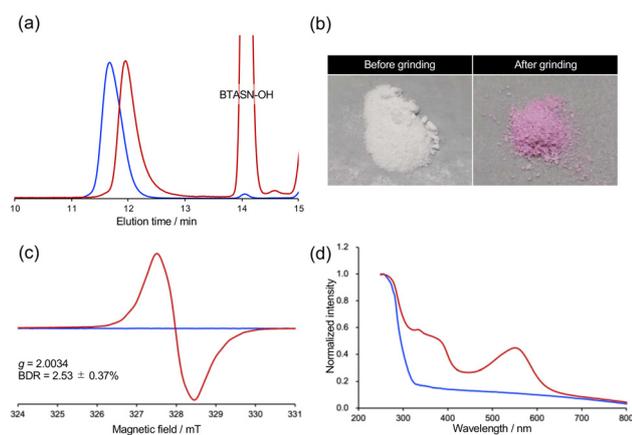
Excited state studies

Interestingly, TAAN radicals, generated by the homolytic cleavage of the central C–C bond in **BTASN**, did not exhibit fluorescence under UV irradiation, despite their structural similarity to fluorescent DAAN radicals.[29] Both radicals consist of a methyl radical connected to two aromatic rings and a cyano group. To gain deeper insight into the fluorescence properties of these mechanophores, density functional theory (DFT) and time-dependent DFT (TD-DFT) calculations were performed for the corresponding DAAN and TAAN radicals (Fig. 4 and Fig. S44, 46, Tables S1, 2). For the DAAN radical, the $D_1 \rightarrow D_0$ transition is primarily attributed to the β-SUMO(67) → β-HOMO(66) transition (96%) (Fig. 4a and Fig. S45, Table S2). In contrast, the $D_1 \rightarrow D_0$ transition of the TAAN radical is mainly attributed to the β-SUMO(91) → β-HOMO(90) transition (77%) (Fig. 4b and Fig. S24, Table S1). The corresponding orbital transition in the DAAN radical is a π–π* transition, which is allowed, and there are no significant changes in the orbital characteristics between the D_0 and D_1 states. However, for the TAAN radical, the n-orbital (HOMO−1(89) in the D_0 state) becomes the HOMO(90) in the D_1 state. This transition is an n–π* transition, which is symmetry-forbidden, and its contribution to the $D_1 \rightarrow D_0$ transition is substantial. This difference likely accounts for the absence of fluorescence in the TAAN radical. The study of fluorescence in radical species provides an important perspective on their electronic structures and excited-state dynamics,[60] and the present findings contribute to a deeper understanding of the fundamental principles governing fluorescent radical molecules.

Fig. 3 (a) GPC profiles of **BTASN-PMMA-H** before (blue line) and after the exchange reaction (red line). (b) Pictures, (c) EPR spectra, and (d) UV-vis spectra of **BTASN-PMMA-H** before (blue lines) and after ball-milling (red lines).


Fig. 4 The molecular orbitals of the corresponding (a) DAAN and (b) TAAN radicals (unrestricted cam-B3LYP/6-311+G(d,p)//unrestricted B3LYP/6-31G(d,p)). The values below the structure represent orbital energy (eV).

Revisit of RSE *vs.* Hammett constant and its scope and limitation: thermal tolerance of RMs consisting of acyclic radicals

RMs composed of dimers of the same radical can be classified into two main radical types of parent skeletons (Fig. 5a). Type A comprises acyclic radicals, whereas type B comprises cyclic radicals. The corresponding radicals of TASN,[28] BTASN and bisarylcyanoacetate (BiACA)[34] as well as diaryltetracyanoethane (DATCE) reported by Sakamaki and Winter *et al.*[61,62] are classified as type A (Fig. 5a). Type B features a methyl radical incorporated into a cyclic skeleton (Fig. 5a), and the corresponding radicals of difluorenylsuccinonitrile (DFSN),[31] 9,9′-bis(4,6-diphenyl-2-triazyl)-9,9′-bifluorene (BTAF), 9,9′-bis(5-methyl-2-pyridyl)-9,9′-bifluorene (BPyF)[33] and diarylbibenzofuranone (DABBF)[28] are classified as type B.

Previously, we reported the prediction of the thermal tolerance of RMs with the same molecular skeleton, based on RSE and the Hammett constant.[34] Building on this approach, this study demonstrates the potential for predicting the thermal tolerance of type A of RMs with different molecular skeletons. One of the parent skeletons in type A features a methyl radical that is sandwiched between one cyano group and one aryl group (Fig. 5b). The corresponding radicals of TASN, BTASN, BiACA and DATCE are classified as the parent skeleton among the type A radicals (Fig. 5b). As shown in Fig. 6, the RSE values of the corresponding radicals of the parent skeletons become lower as the Hammett constant increases. Furthermore, as shown in Fig. 7a, the logarithm values of the dissociation constants (K_d) of the RMs including DAANs, TAAN and ACAs linearly increase
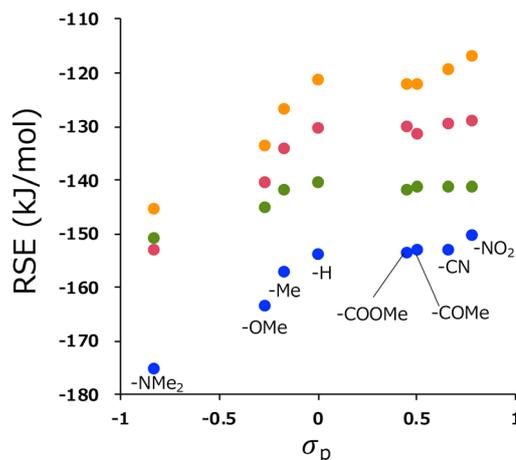
Fig. 6 Plot of RSE against the Hammett constant. Blue circle: ADCM radicals,[34] green circle: DAAN radicals,[34] pink circle: TAAN radicals, and orange circle: ACA radicals.[34] DFT calculations were performed at the unrestricted B3LYP/6-31++G(d,p) level.

with increasing RSE values (please see the synthetic part of SI, Fig. S36–S39 and Table S3). The coefficient of determination (R^2) of the linear fit is 0.8406. The dissociation of the central C–C bond of aryl dicyanomethyl (ADCM) dimers classified as the same parent skeleton is fast, and the corresponding radicals are stable under ambient conditions.[62] Fig. 7b shows the plots in which the $\ln K_d$ values calculated from the reported binding constants and the RSE values of ADCMs were added to the plots in Fig. 7a. As we expected, the values of $\ln K_d$ linearly increased with the RSE values as in the case of Fig. 7a, and the R^2 value of the linear fit was relatively good ($R^2 = 0.6476$). The decrease in the R^2 value is likely due to the fact that the values of ADCMs were measured in methanol or toluene at 50 °C, which is different from our experimental conditions. These results indicate that, within the classification of type A RMs, the thermal stability of RMs increases in the order BiACA > BTASN > TASN > ADCM structures owing to the generation of the corresponding radicals having lower RSE values, and that the introduction of electron-withdrawing groups enhances the thermal stability of RMs across different molecular skeletons.

We reported that the relationship between RSE/thermodynamic stability and the thermal tolerance of RMs can be explained by the Hammond–Leffler postulate, which describes the transition-state (TS) geometry in an elementary step related to reactants, intermediates, and products.[34] However, at present, it is still challenging to provide a consistent explanation for acyclic and cyclic radical systems as well as non-dimer type RMs based solely on RSE and substituent effects. For example, DFSN and BTAF classified as type B show enough thermal tolerance for application to ATRP, although the values of RSEs are almost the same as DABBF derivatives, whose central C–C bond undergoes homolysis even under ambient conditions.[31,33] We believe that this discrepancy is likely due to the fact that the transition state structures are entirely different between cyclic radicals, which can adopt highly planar structures, and acyclic radicals, which cannot.
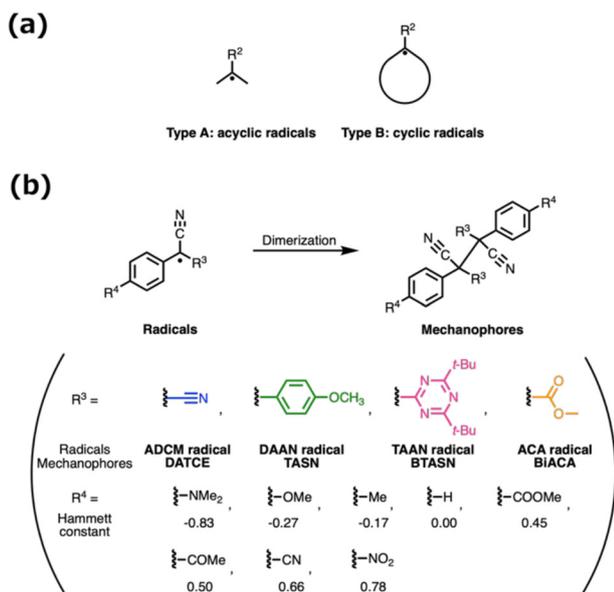
Fig. 5 (a) Classification of the corresponding radicals generated by RMs: type A: acyclic radicals and type B: cyclic radicals. (b) Representative chemical structures of the acyclic radicals (type A) with the parent skeleton consisting of a methyl radical sandwiched between one cyano group and one aryl group. ADCM and ACA radicals stand for aryldicyanomethyl and arylcyanoacetate radicals, respectively.
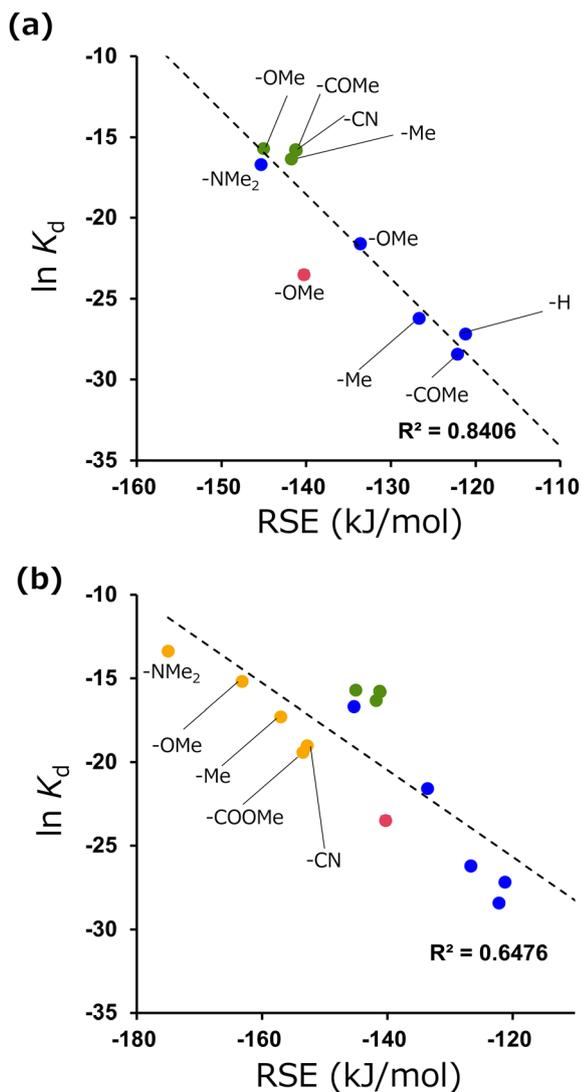
Fig. 7 Plot of RSE values and $\ln K_d$ of RMs. The dotted line and R^2 indicate an approximated curve and coefficient of determination. Blue circle: ADCM radicals, green circle: DAAN radicals, pink circle: TAAN radicals, and orange circle: ACA radicals. These chemical structures are shown in Fig. 5b, in which the color corresponds to the filled circles.

Furthermore, diarylacetonitrile-α-carboxylic ester (DAANAC) is also an RM consisting of a DAAN radical and an alkoxycarbonyl radical, which shows exceptional thermal stability.[63] DAANAC is not a dimer of radicals and the driving force for the generation of radicals might be decarboxylation generating carbon dioxide gas. Further research into the inherent understanding of the origin of thermal stability of radical mechanophores is underway in our group.

Conclusions

We demonstrated the synthesis and mechanochemical reactivity of **BTASN-OMe**, a triazine-substituted TASN-type mechanophore with enhanced thermal stability. Computational analyses, including RSE, CoGEF calculations, and MD simulations, revealed that the introduction of electron-withdrawing triazine rings significantly improved thermal resistance compared with conventional **TASN** while maintaining mechanical responsiveness. Experimental thermal tolerance tests supported these findings, showing that **BTASN-OMe** exhibited a dissociation ratio approximately 64 times lower than **TASN**. The high thermal stability enabled the successful ATRP of MMA using a bifunctional ATRP initiator derived from **BTASN-OMe**. The resulting polymers exhibited sufficient mechanical response while maintaining thermal stability. The difference in fluorescence behavior between TAAN and DAAN radicals was attributed to the nature of their electronic transitions: TAAN undergoes a forbidden n–π* transition due to orbital changes involving the nitrogen atom of the triazine ring in the D_1 state, while DAAN undergoes an allowed π–π* transition. Furthermore, these results allowed us to predict the thermal tolerance of RMs consisting of the dimer of acyclic radicals through RSE values, even with different molecular skeletons. Overall, **BTASN-OMe** represents a significant advancement in the design of thermally stable mechanophores, containing enhanced thermal tolerance with robust mechanical responsiveness. This dual functionality broadens the potential applications of responsive polymer materials in fields requiring both mechanical reactivity and thermal endurance.

Conflicts of interest

There are no conflicts of interest to declare.

Data availability

Data supporting this article have been included in the supplementary information (SI). Supplementary information: synthetic procedures of compounds and polymers and their NMR, IR, GPC, and EPR data as well as details of the computations. See DOI: https://doi.org/10.1039/d5py01088h.

Acknowledgements

References

1 Y. Yang and M. W. Urban, *Chem. Soc. Rev.*, 2013, **42**, 7446.
2 S. Shahi, H. Roghani-Mamaqani, R. Hoogenboom, S. Talebi and H. Mardani, *Chem. Mater.*, 2022, **34**, 468.

3 K. Imato, M. Nishihara, T. Kanehara, Y. Amamoto, A. Takahara and H. Otsuka, *Angew. Chem., Int. Ed.*, 2012, **51**, 1138.

4 T. Matsuda, R. Kawakami, R. Namba, T. Nakajima and J. P. Gong, *Science*, 2019, **363**, 504.

5 K. Seshimo, H. Sakai, T. Watabe, D. Aoki, H. Sugita, K. Mikami, Y. Mao, A. Ishigami, S. Nishitsuji, T. Kurose, H. Ito and H. Otsuka, *Angew. Chem., Int. Ed.*, 2021, **60**, 8406.

6 D. A. Davis, A. Hamilton, J. Yang, L. D. Cremar, D. Van Gough, S. L. Potisek, M. T. Ong, P. V. Braun, T. J. Martínez, S. R. White, J. S. Moore and N. R. Sottos, *Nature*, 2009, **459**, 68.

7 Y. Chen, A. J. H. Spiering, S. Karthikeyan, G. W. M. Peters, E. W. Meijer and R. P. Sijbesma, *Nat. Chem.*, 2012, **4**, 559.

8 J. R. Hemmer, C. Rader, B. D. Wilts, C. Weder and J. A. Berrocal, *J. Am. Chem. Soc.*, 2021, **143**, 18859.

9 T. Wang, N. Zhang, J. Dai, Z. Li, W. Bai and R. Bai, *ACS Appl. Mater. Interfaces*, 2017, **9**, 11874.

10 Y. Chen, G. Mellot, D. Van Luijk, C. Creton and R. P. Sijbesma, *Chem. Soc. Rev.*, 2021, **50**, 4100.

11 M. B. Larsen and A. J. Boydston, *J. Am. Chem. Soc.*, 2013, **135**, 8189.

12 G. R. Gossweiler, G. B. Hewage, G. Soriano, Q. Wang, G. W. Welshofer, X. Zhao and S. L. Craig, *ACS Macro Lett.*, 2014, **3**, 216.

13 X. Hu, T. Zeng, C. C. Husic and M. J. Robb, *J. Am. Chem. Soc.*, 2019, **141**, 15018.

14 H. Shen, M. B. Larsen, A. G. Roessler, P. M. Zimmerman and A. J. Boydston, *Angew. Chem., Int. Ed.*, 2021, **60**, 13559.

15 Y. Lu, H. Sugita, K. Mikami, D. Aoki and H. Otsuka, *J. Am. Chem. Soc.*, 2021, **143**, 17744.

16 K. Suwada, A. W. Ieong, H. L. H. Lo and G. De Bo, *J. Am. Chem. Soc.*, 2023, **145**, 20782.

17 P. Liu, Y.-L. Tseng, L. Ge, T. Zeng, D. Shabat and M. J. Robb, *J. Am. Chem. Soc.*, 2024, **146**, 22151.

18 J. Li, C. Nagamani and J. S. Moore, *Acc. Chem. Res.*, 2015, **48**, 2181.

19 Q. Mu and J. Hu, *Phys. Chem. Chem. Phys.*, 2024, **26**, 679.

20 X. Chen, H. Shen and Z. Zhang, *Chin. J. Chem.*, 2024, **42**, 1418.

21 D. Xu, X. Cheng, W. Liu, Y. Sun, Y. Niu, M. Wang and H. Qian, *Chem. Rev.*, 2026, **126**, DOI: 10.1021/acs.chemrev.5c00789.

22 C. E. Diesendruck, B. D. Steinberg, N. Sugai, M. N. Silberstein, N. R. Sottos, S. R. White, P. V. Braun and J. S. Moore, *J. Am. Chem. Soc.*, 2012, **134**, 12446.

23 C. Nagamani, H. Liu and J. S. Moore, *J. Am. Chem. Soc.*, 2016, **138**, 2540.

24 T. Shiraki, C. E. Diesendruck and J. S. Moore, *Faraday Discuss.*, 2014, **170**, 385.

25 C. E. Diesendruck, G. I. Peterson, H. J. Kulik, J. A. Kaitz, B. D. Mar, P. A. May, S. R. White, T. J. Martínez, A. J. Boydston and J. S. Moore, *Nat. Chem.*, 2014, **6**, 623.

26 L. Chen, R. Nixon and G. De Bo, *Nature*, 2024, **628**, 320.

27 M. J. Robb and J. S. Moore, *J. Am. Chem. Soc.*, 2015, **137**, 10946.

28 K. Imato, A. Irie, T. Kosuge, T. Ohishi, M. Nishihara, A. Takahara and H. Otsuka, *Angew. Chem., Int. Ed.*, 2015, **54**, 6168.

29 T. Sumi, R. Goseki and H. Otsuka, *Chem. Commun.*, 2017, **53**, 11885.

30 K. Ishizuki, H. Oka, D. Aoki, R. Goseki and H. Otsuka, *Chem. – Eur. J.*, 2018, **24**, 3170.

31 H. Sakai, T. Sumi, D. Aoki, R. Goseki and H. Otsuka, *ACS Macro Lett.*, 2018, **7**, 1359.

32 K. Kawasaki, D. Aoki and H. Otsuka, *Macromol. Rapid Commun.*, 2020, **41**, 1900460.

33 H. Sugita, Y. Lu, D. Aoki, H. Otsuka and K. Mikami, *Chem. – Eur. J.*, 2023, **29**, e202203249.

34 Y. Lu, H. Sugita, K. Mikami, D. Aoki and H. Otsuka, *Chem. Sci.*, 2023, **14**, 8792.

35 K. Imato, T. Kanehara, S. Nojima, T. Ohishi, Y. Higaki, A. Takahara and H. Otsuka, *Chem. Commun.*, 2016, **52**, 10482.

36 S. Kato, K. Ishizuki, D. Aoki, R. Goseki and H. Otsuka, *ACS Macro Lett.*, 2018, **7**, 1087.

37 F. Hoshino, T. Kosuge, D. Aoki and H. Otsuka, *Mater. Chem. Front.*, 2019, **3**, 2681.

38 T. Kosuge, X. Zhu, V. M. Lau, D. Aoki, T. J. Martinez, J. S. Moore and H. Otsuka, *J. Am. Chem. Soc.*, 2019, **141**, 1898.

39 H. Sakai, D. Aoki, K. Seshimo, K. Mayumi, S. Nishitsuji, T. Kurose, H. Ito and H. Otsuka, *ACS Macro Lett.*, 2020, **9**, 1108.

40 Y. Mao, Y. Kubota, T. Kurose, A. Ishigami, K. Seshimo, D. Aoki, H. Otsuka and H. Ito, *Macromolecules*, 2020, **53**, 9313.

41 Y. Mao, Y. Kubota, J. Gong, T. Kurose, A. Ishigami, K. Seshimo, T. Watabe, D. Aoki, H. Otsuka and H. Ito, *Macromolecules*, 2021, **54**, 8664.

42 Y. Mao, Y. Kubota, R. Feng, J. Gong, A. Ishigami, Y. Kobayashi, T. Watabe, D. Aoki, H. Otsuka and H. Ito, *Macromolecules*, 2022, **55**, 3948.

43 T. Watabe, D. Aoki and H. Otsuka, *Macromolecules*, 2022, **55**, 5795.

44 K. Ishizuki, A. Takahashi and H. Otsuka, *Macromol. Rapid Commun.*, 2025, **46**, 2400812.

45 M. K. Beyer, *J. Chem. Phys.*, 2000, **112**, 7307.

46 M. Klein, C. C. Husic, D. P. Kovács, N. J. Choquette and M. J. Robb, *J. Am. Chem. Soc.*, 2020, **142**, 16364.

47 S. Yoon, J. H. Choi, B. J. Sung, J. Bang and T. A. Kim, *NPG Asia Mater.*, 2022, **14**, 61.

48 S. Takamoto, C. Shinagawa, D. Motoki, K. Nakago, W. Li, I. Kurata, T. Watanabe, Y. Yayama, H. Iriguchi, Y. Asano, T. Onodera, T. Ishii, T. Kudo, H. Ono, R. Sawada, R. Ishitani, M. Ong, T. Yamaguchi, T. Kataoka, A. Hayashi, N. Charoenphakdee and T. Ibuka, *Nat. Commun.*, 2022, **13**, 2991.

49 L. Hintermann, L. Xiao and A. Labonne, *Angew. Chem., Int. Ed.*, 2008, **47**, 8246.

50 S. Kato, D. Aoki and H. Otsuka, *Polym. Chem.*, 2019, **10**, 2636.

51 S. Kato, S. Furukawa, D. Aoki, R. Goseki, K. Oikawa, K. Tsuchiya, N. Shimada, A. Maruyama, K. Numata and H. Otsuka, *Nat. Commun.*, 2021, **12**, 126.

52 S. Kato, D. Aoki and H. Otsuka, *ACS Appl. Polym. Mater.*, 2021, **3**, 594.

53 S. Kato, D. Aoki, K. Oikawa, K. Tsuchiya, K. Numata and H. Otsuka, *ACS Macro Lett.*, 2021, **10**, 623.

54 S. Kato, D. Aoki and H. Otsuka, *Chem. Lett.*, 2021, **50**, 1223.

55 M. Van Galen, J. P. Kaniraj, B. Albada and J. Sprakel, *J. Phys. Chem. C*, 2022, **126**, 1215.

56 N. Li, Z. Cui, X. Yue, Y. Zhang, Z.-H. Ren and Z.-H. Guan, *Sens. Actuators, B*, 2024, **404**, 135266.

57 Y. Zhu, M. Wang, J. Huang, H. Mi, Z. Xu, F. Wu, L. Chen, H. Yang and Y. Chen, *Macromolecules*, 2024, **57**, 8329.

58 C. Zhang, N. Li, J. Ren, H. Ouyang, X. Dong, Z. Cui, Z.-H. Ren and Z.-H. Guan, *Chem. Mater.*, 2024, **36**, 10474.

59 Y. Xu, Y. Huang, J. Wang, S. Huang, H. Yang and Q. Li, *Angew. Chem., Int. Ed.*, 2025, **64**, e202423584.

60 A. Mizuno, R. Matsuoka, T. Mibu and T. Kusamoto, *Chem. Rev.*, 2024, **124**, 1034.

61 T. Kobashi, D. Sakamaki and S. Seki, *Angew. Chem., Int. Ed.*, 2016, **55**, 8634.

62 J. P. Peterson, M. R. Geraskina, R. Zhang and A. H. Winter, *J. Org. Chem.*, 2017, **82**, 6497.

63 Y. Uchida, H. Sugita, A. Takahashi and H. Otsuka, *J. Am. Chem. Soc.*, 2025, **147**, 44686.